EULERIAN MODELLING OF ATOMISATION IN TURBULENT FLOWS

Novid Beheshti and Alexey A. Burluka

School of Mechanical Engineering
University of Leeds, Leeds, LS2 9JT, UK
N.Beheshti@leeds.ac.uk, A.A.Burluka@leeds.ac.uk

ABSTRACT

This work is devoted to verify the ability of the Eulerian model of [1] in prediction of the effects of *a) liquid properties*, such as density and surface tension, *b) the injector regimes*, such as variations in liquid and gas velocities and *c) the injector exit velocity profiles* on air-assisted atomisation. Here it is shown that this model is predicting these trends very well in comparison with a number of different empirical correlations gathered in [3].

Also, a new model within the same Eulerian framework, for the prediction of *slip velocities* is proposed and assessed against experimental data of a co-axial atomiser which shows good agreement with the measurements.

INTRODUCTION

In spite of its importance, the description of atomisation remains largely at the level of semi-empirical formulae adjusted for a particular type of injector. As an attempt to provide a reliable means for atomisation prediction, this work explores the predictive ability of the recently proposed Eulerian model of [1] in a wide range of operating conditions compared with the empirical correlations gathered in [3] for plain-jet air-assisted atomisers. Also, effect of nozzles exit velocity profiles on extent of atomisation is investigated comparing the model results with the co-axial atomiser measurements of [5, 6]. Then a new Eulerian model for prediction of slip velocity is proposed in conjunction with the same atomisation model and is verified by comparison with experimental data of another co-axial atomiser [7].

ATOMISATION MODEL

Atomisation model used in this work consists of two transport equations, one is for the mass fraction of liquid phase $\tilde{Y}_{liq}$ and the other is for is the mean surface area of the gas-liquid interface per unit mass of two-phase media $\tilde{s}$, [1]. These equations are:

$$\frac{\partial \bar{r}\tilde{Y}_{liq}}{\partial t}+\frac{\partial \bar{r}\tilde{u}_j\tilde{Y}_{liq}}{\partial x_j}=\frac{\partial}{\partial x_j}\bar{r}\frac{D_T}{Sc_{liq}}\frac{\partial \tilde{Y}_{liq}}{\partial x_j}-\dot{m}_{vap}\bar{r}\tilde{s} \tag{1}$$

$$\frac{\partial \bar{r}\tilde{s}}{\partial t}+\frac{\partial \bar{r}\,\tilde{u}_j\tilde{s}}{\partial x_j}=\frac{\partial}{\partial x_j}\bar{r}\frac{D_T}{Sc_s}\frac{\partial \tilde{s}}{\partial x_j}+\frac{\bar{r}\tilde{s}}{t_c}(1-\frac{\tilde{s}}{\tilde{s}_{eq}}) \tag{2}$$

where $\dot{m}_{vap}$ is the mean vaporisation rate per unit surface, D_T is the turbulent diffusivity, t_c is the rate of surface production which is here taken proportional to the turbulence time scale:

$$t_c=C_1\frac{\tilde{k}}{\tilde{e}} \tag{3}$$

In Eq. (2) $\tilde{s}_{eq}$ is the liquid surface area defined in terms of the droplet radius characterising a monodisperse spray at equilibrium with local turbulence, [1, 4]:

$$\tilde{s}_{eq}=\frac{3\tilde{Y}_{liq}}{r_{liq}r_{eq}} \qquad r_{eq}=C_r\left(\frac{\bar{r}\tilde{Y}_{liq}}{r_{liq}}\right)^{2/15}\left(\frac{h}{e\,r_{liq}}\right)^{3/5} \tag{4}$$

The atomisation model, Eqs. (1) and (2), requires turbulent diffusivity and integral scale t_c and the standard *k-e* model is used to calculate these variables. Compared to homogeneous gaseous flow modelling of two-phase mixture requires different equation of state for the mean density:

$$\frac{1}{\bar{r}} = \frac{\tilde{Y}_{liq}}{r_l} + \frac{(1-\tilde{Y}_{liq})}{r_g} \tag{5}$$

and account of liquid incompressibility:

$$\bar{p} = \frac{\bar{r}(1-\tilde{Y}_{liq})R_g T_g}{1-\bar{r}\,\tilde{Y}_{liq}/r_l} \tag{6}$$

In this approach, two-phase mixture is considered as a single continuum therefore the equations of motion are the usual Favre-averaged Reynolds equations. The governing set of equations was solved with standard finite-volume method [4] employing iterative methods. Large density variations made necessary use of rather small under-relaxation factors to avoid divergence of iterations.

APPLICATION TO AIR-ASSISTED ATOMISATION

The model described above was applied for simulation of plain-jet air-assisted atomisation. This case has a very simple flow geometry and is relatively well studied experimentally [5, 6, 7].

First the model is applied for investigation of influence which the velocity profile at the injector exit may exert upon the extent of atomisation. Atomisation of a round water jet by a high velocity co-axial air flow [5,6] was chosen for this purpose as a test case. The first step in modelling consisted in finding the values of coefficients C_1 and C_r in Eqs. (3) and (4) providing drop sizes in a good agreement with measurements at one particular set of conditions; so found constants are C_r = 0.73, and C_1 = 4.38 and these values were then kept unchanged for all subsequent simulations.

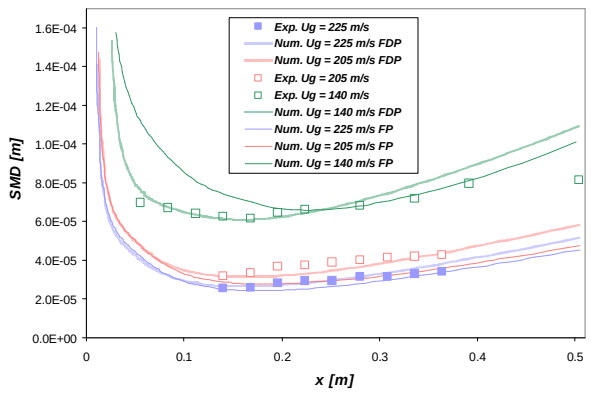

Fig. 1. Axial distribution of droplet SMD for different air velocities compared to measured values

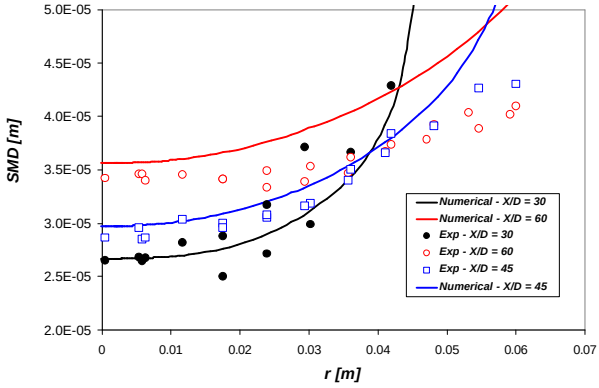

Fig. 2. Radial distribution of droplet SMD for air velocity of 225m/s compared to measured values

Figure 1 presents the comparison of calculated droplet *SMD* on the flow symmetry axis with the values measured in [5, 6] for different air velocities. The calculations performed assuming uniform velocity profiles at the injector exit are shown in thin lines (FP for flat profile); thick lines show the results obtained with the exit profiles corresponding to fully-developed round pipe turbulence (FDP). For the strongest atomisation, $u_{o,g}$ = 225 m/s the exit velocity profile has very limited effect, however, its importance increases with decreasing air velocity. For small gas velocity, use of uniform velocity profile results in primary atomisation rate significantly slower than it was observed in [6], this is hardly surprising as the nozzle lengths used in measurements correspond to a fully developed pipe flow. It is appropriate to note that in the model used in this work the primary atomisation rate is governed solely by turbulent straining of the liquid surface. The turbulence generation is quite sensitive to the exit velocity profile and this explains unrealistically slow primary atomisation predicted with an unrealistic injector exit conditions. Unfortunately, no turbulence measurements are available for this case and this does not allow a direct verification of *k-e* model predictions. However, the spread rate of the jet has been predicted with the reasonable accuracy. This can be seen in Fig. (2) which presents the radial profiles of *SMD* for air jet exit velocity of 225 m/s calculated with a fully-developed profile against the measurements [5].

Agreement obtained for one limited set of conditions can always be fortuitous; the predictive model must be able to describe the influence of all relevant parameters varied over as wide range as it can be encountered in practice. For air-assisted atomisation process the review [3] presented the summary of large number of experiments performed with different injectors. The findings of [3] are presented in terms of power-law dependency of an average spray *SMD* upon a parameter value suggesting a tentative “global” correlation for prefilming atomisation as:

$$SMD = \left[1 + \frac{\dot{m}_l}{\dot{m}_g}\right]\left[0.073 D_l^{2/5}\left(\frac{h}{r_g u_{0,g}^2}\right)^{3/5}\left(\frac{r_l}{r_g}\right)^{1/10} + 0.015\left(\frac{m_l^2 D_l}{h r_l}\right)^{1/2}\right] \quad (7)$$

At the same time, it was also noticed that spray generated by a plain-jet atomiser is characterised with similar dependencies except possibly a very slight independent influence of the liquid mass flow rate not observed for a prefilming atomiser [3]. Two additive terms in the above equation come from different atomisation regimes and the second term containing the liquid viscosity is thought to be unimportant for low-viscosity liquids such as water or kerosene. The model we employ here is developed for high Reynolds numbers, in which case neither gas nor liquid viscosity should be determining the spray properties. Indeed, the present model is insensitive to the values of the liquid viscosity therefore the comparison with the correlations published in [3] is restricted to the low-viscosity liquids such as water or kerosene. Therefore, the comparisons below employ values of exponents corresponding to the first term of the Eq. (7) only. It should also be noted that though the Eq. (7) was shown in [3] to be a successful approximation to a number of observations the individual sets of experiments reveal significant differences in the exponents values, see the Tab.1.

Tab. 1. Predicted and empirical measured exponents for droplet SMD

factor	Model predicted exponent	Measured exponent, [3]
surface tension	0.6	0.5 to 0.7
air velocity	-1.7	-1.33 to -1.0
liquid density	-0.52 to -0.57	-0.5 to -0.35
air density	-0.1 to -0.67	-0.57 to -0.3

Figure 3 presents calculated *SMD* values obtained with variations of the surface tension h by a factor of 80. The surface tension is reduced at conditions approaching the liquid critical state, e.g. with temperature and pressure rise. Distribution of temperature is usually very non-uniform inside a typical industrial combustion chamber; therefore a predictive atomisation model should be able to account for wide variations of h. The modelling results in $SMD \sim h^{3/5}$ in an excellent agreement with Eq. (7) while experimentally observed exponents range between 0.5 and 0.7, [3].

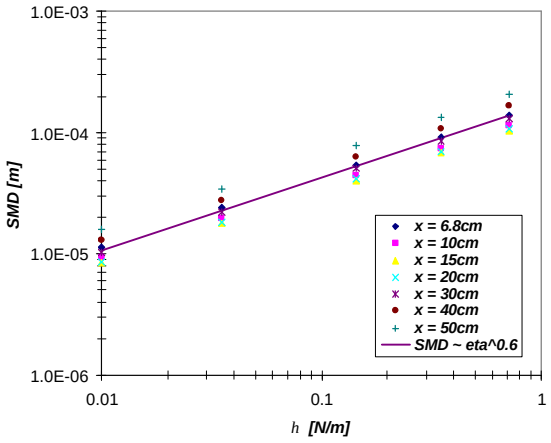

Fig. 3. Power-law dependency of droplet SMD on surface tension h

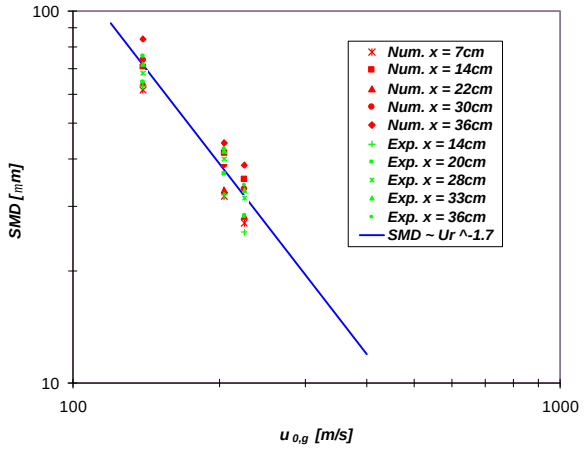

Fig. 4. Power-law dependency of droplet SMD on air velocity $u_{0,g}$

Turbulence is generated by the shear between high velocity co-flow gas and usually low velocity liquid jet. The gas velocity affects the atomisation strongly and the measured corresponding exponent ranges from -1.0 to -1.33, [3] while the Eq. (7) results in the exponent value of -2.2. The modelling predicts $SMD \sim u_g^{-1.7}$, see Fig. 4. In calculations it was found that the variations in gas velocity change considerably the flow pattern and turbulence properties, it also changes a number of factors such as momentum and mass flux ratios in an interdependent way. It would be desirable to have some data where the effects of the air velocity are isolated.

Figures 5 and 6 present the droplet *SMD* calculated using different values of liquid and air/gas densities. It can be seen clearly that the exponents a_l and a_g in an expression $SMD \sim r_l^{a_l} \cdot r_g^{a_g}$ are not constant over the entire flow field, moreover, such power-law correlation may be poor near the injector but is quite adequate further downstream. The Eq. (7) would yield $SMD \sim r_l^{11/10}$ if the liquid density is changed provided all other variables are kept the same and $SMD \sim r_l^{1/10}$ if it would be changed provided the liquid/gas mass flux ration is kept constant. The calculation yields *SMD* approximately independent of liquid density near the injector in line with the latter expression, if the liquid density is greater than a certain value. If r_l is below approximately 100 kg/m^3, *SMD* scales approximately with the inverse of the density square root, see points taken at x = 10cm downstream in Fig. 5. At the same time, further downstream x = 50cm

positions reveal $SMD \sim r_l^{0.57}$. Similarly, near the injector $SMD \sim r_g^{0.67}$ while further downstream $SMD \sim r_g^{0.1}$, see Fig. 6.

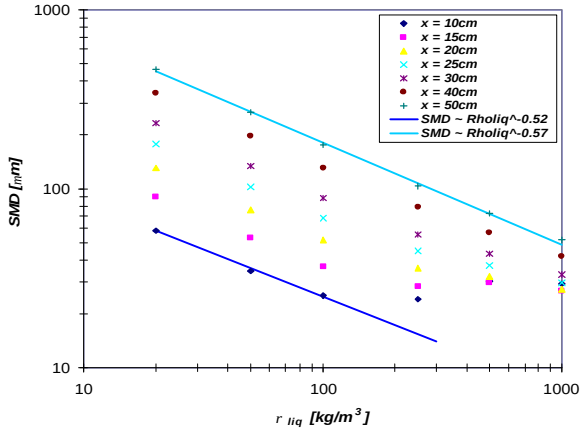

Fig. 5. Power-law dependency of droplet SMD on liquid density r_{liq}

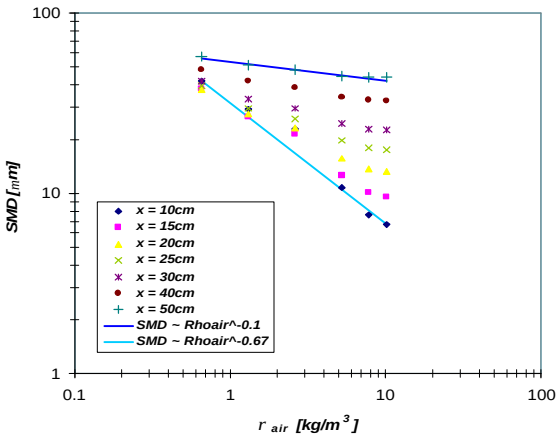

Fig. 6. Power-law dependency of droplet SMD on air density r_{air}

The observed lack of a single value of an exponent in $SMD \sim r_l^{a_l} \cdot r_g^{a_g}$ suitable for the entire flow field deserves a comment. Indeed, a vast number of similar formulae have been proposed both for droplet size [3] and liquid core length [2]. Practically, a change in either phase density will entrain a change in flow details, in particular, turbulence generation, henceforth, it would be very difficult to isolate effects caused solely by the density change. The summary tables in the review [3] show clearly much larger scatter in values of density exponents, so a_l varies from 0 to 0.5 for prefilming and even changes the sign ranging from 0 to -0.5 for plain jet atomisers. If to take into account that, first, in most experiments the variation in r_l is rather limited and second, that the exponent a_l depends, according to our calculations, on location of observation† then the magnitude of scatter in data summarised in [3] is hardly surprising. Similarly, decrease in air density results in poorer atomisation [3], $-1.0 \le a_g \le -0.25$, the trend perfectly captured by the present model. In other words, the present model assumes that the only mechanism for the primary atomisation is the flow turbulence and the liquid or gas density affects the atomisation quality only as far as it affects the turbulence; and assuming this it produces rather good agreement with experiments. This hypothesis can also explain effects of the nozzle geometry [2, 3].

From the above, one can conclude that the present model provides realistic description of air-assisted atomisation and influence of all major factors except liquid viscosity.

RELATIVE MOTION BETWEEN LIQIUD AND GAS

In its original formulation the model had no provision for determining the relative motion between gas and liquid. In fact, under the assumptions of the model [1] the relative motion has no effect on the model equations as the atomisation rate is defined by the turbulence and the mixture is considered as a single continuum. However, there may be some circumstances where this relative motion may become important, e.g. vaporisation rate [8] depends on gas velocity relative to the droplet. It proved quite easy to obtain an equation for the slip velocity, which is the relative velocity between gas and liquid, within the framework of the present model. This section is devoted to the derivation and application of this newly derived equation to air-assisted atomisation.

Momentum of the liquid in the unit volume can be written as $r_{liq}\Lambda\overline{u}_{i,l} = \overline{r}\tilde{Y}_{liq}\overline{u}_{i,l}$ where L is volumetric liquid fraction defined as $\Lambda = \dfrac{\overline{r}\tilde{Y}_{liq}}{r_l}$. Following usual practice in turbulence modelling, the convection and diffusion terms in the transport equation for momentum of the liquid are $\tilde{u}_j \dfrac{\partial}{\partial x_j}\overline{r}\tilde{Y}_{liq}\overline{u}_{i,l}$ and $\dfrac{\partial}{\partial x_j}D_T\dfrac{\partial}{\partial x_j}\overline{r}\tilde{Y}_{liq}\overline{u}_{i,l}$ respectively. The source term for the liquid momentum is caused by the momentum exchange S between liquid and gas. Also, a pressure gradient would accelerate the liquid and gas differently because of their different densities. Consistently with the equation of state, Eq. (5), the total rate of change of momentum of the mixture $-\dfrac{1}{\overline{r}}\dfrac{\partial\overline{P}}{\partial x_i}$ should be split into liquid and gas shares as $-\dfrac{\tilde{Y}_{liq}}{r_l}\dfrac{\partial\overline{P}}{\partial x_i}$ and $-\dfrac{1-\tilde{Y}_{liq}}{r_g}\dfrac{\partial\overline{P}}{\partial x_i}$, respectively. So, the transport equation for the momentum of liquid becomes:

$$\frac{\partial}{\partial t}\overline{r}\tilde{Y}_{liq}\overline{u}_{i,l} + \frac{\partial}{\partial x_j}\tilde{u}_j(\overline{r}\tilde{Y}_{liq}\overline{u}_{i,l}) = \frac{\partial}{\partial x_k}D_T\frac{\partial\overline{r}\tilde{Y}_{liq}\overline{u}_{i,l}}{\partial x_k} + S - \frac{\tilde{Y}_{liq}}{r_l}\frac{\partial\overline{P}}{\partial x_i} \qquad (8)$$

†Or, rather this exponent would depend on whether the coalescence becomes of importance at that location.

Similarly, momentum of gas per unit volume is $\rho_g(1-\Lambda)\bar{u}_{i,g} = \rho_g(1-\frac{\bar{\rho}\tilde{Y}_{liq}}{\rho_l})\bar{u}_{i,g}$ and its transport equation multiplied by $\frac{\rho_l}{\rho_g}$ could be written as:

$$\frac{\partial}{\partial t}(\rho_l - \bar{\rho}\tilde{Y}_{liq})\bar{u}_{i,g} + \frac{\partial}{\partial x_j}\tilde{u}_j(\rho_l - \bar{\rho}\tilde{Y}_{liq})\bar{u}_{i,g} = \frac{\partial}{\partial x_k}D_T\frac{\partial(\rho_l - \bar{\rho}\tilde{Y}_{liq})\bar{u}_{i,g}}{\partial x_k} - \frac{\rho_l}{\rho_g}S - \frac{\rho_l(1-\tilde{Y}_{liq})}{\rho_g^2}\frac{\partial\bar{P}}{\partial x_i} \quad (9)$$

Subtracting Eq. (8) from Eq. (9) results in:

$$\frac{\partial}{\partial t}\bar{\rho}\tilde{Y}_{liq}(\bar{u}_{i,g}-\bar{u}_{i,l}) + \frac{\partial}{\partial x_j}\tilde{u}_j\bar{\rho}\tilde{Y}_{liq}(\bar{u}_{i,g}-\bar{u}_{i,l}) - \frac{\partial}{\partial x_k}D_T\frac{\partial\bar{\rho}\tilde{Y}_{liq}(\bar{u}_{i,g}-\bar{u}_{i,l})}{\partial x_k} = -S(\frac{\rho_l}{\rho_g}+1)$$
$$-\rho_l\left(\frac{\partial}{\partial t}\bar{u}_{i,g} + \frac{\partial}{\partial x_j}\tilde{u}_j\bar{u}_{i,g} - \frac{\partial}{\partial x_k}D_T\frac{\partial\bar{u}_{i,g}}{\partial x_k}\right) - \frac{\rho_l(1-Y_{liq})}{\rho_g^2}\frac{\partial P}{\partial x_i} \quad (10)$$

The pressure term can be simplified considering that liquid density is usually much larger than that of the gas and it can be shown that the second term on the right hand side is:

$$\rho_l\left(\frac{\partial}{\partial t}\bar{u}_{i,g} + \frac{\partial}{\partial x_j}\tilde{u}_j\bar{u}_{i,g} - \frac{\partial}{\partial x_k}D_T\frac{\partial\bar{u}_{i,g}}{\partial x_k}\right) = \left(\bar{u}_{i,g}\dot{m}_{vap} + S\frac{\rho_l}{\rho_g}\right)/(1-\Lambda) \quad (11)$$

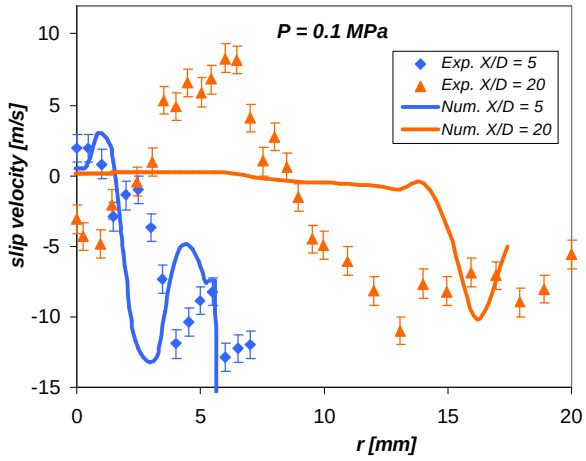

Fig. 7. Comparison of predicted and measured radial profiles of axial slip velocity at 0.1MPa

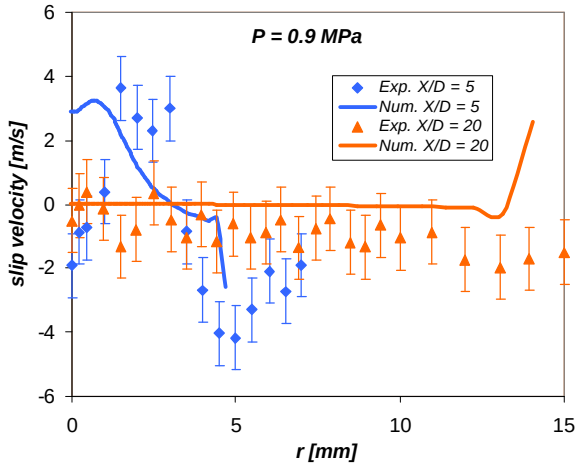

Fig. 8. Comparison of predicted and measured radial profiles of axial slip velocity at 0.9MPa

In order to find the momentum exchange S, we presume that there is a turbulent boundary layer of gas developing on a surface of liquid parcel of characteristic size d. Then the velocity gradient and the thickness d of this boundary layer can be estimated as $C_\Delta\frac{\bar{u}_{i,g}-\bar{u}_{i,l}}{d}$ and $d \sim d.\mathrm{Re}_d^{-1/2} = d\left[\frac{(\bar{u}_{i,g}-\bar{u}_{i,l})d}{u_g}\right]^{-1/2}$, respectively. Consequently, the resulting shear stress on the liquid surface is $u_g\rho_g\left|\frac{\partial u}{\partial n}\right| \approx C_\Delta\frac{(\bar{u}_{i,g}-\bar{u}_{i,l})^{3/2}u_g^{1/2}\rho_g}{d^{1/2}}$ and the total friction force per unit volume is $C_\Delta\bar{\rho}\tilde{s}\frac{(\bar{u}_{i,g}-\bar{u}_{i,l})^{3/2}u_g^{1/2}\rho_g}{d^{1/2}}$. Here d is taken as $\frac{6\tilde{Y}_{liq}}{\tilde{s}\rho_l}$ which is the spray *SMD*. Therefore, the momentum exchange term is written as:

$$S = C_\Delta\bar{\rho}\frac{\rho_g\rho_l^{1/2}u_g^{1/2}\tilde{s}^{3/2}}{\tilde{Y}_{liq}^{1/2}}(\bar{u}_{i,g}-\bar{u}_{i,l})^{3/2} \quad (12)$$

Now, substitution of Eqs. (11) and (12) into Eq. (10) gives the final form of the transport equation for the inter-phase motion momentum as:

$$\frac{\partial}{\partial t}\overline{r}\tilde{Y}_{liq}(\overline{u}_{i,g}-\overline{u}_{i,l})+\frac{\partial}{\partial x_j}\tilde{u}_j\overline{r}\tilde{Y}_{liq}(\overline{u}_{i,g}-\overline{u}_{i,l})=\frac{\partial}{\partial x_k}\frac{D_T}{Sc_m}\frac{\partial\overline{r}\tilde{Y}_{liq}(\overline{u}_{i,g}-\overline{u}_{i,l})}{\partial x_k}-\frac{r_l}{r_g^{\,2}}(1-\tilde{Y}_{liq})\frac{\partial P}{\partial x_i}$$
$$-C_\Delta\frac{r_l^{3/2}u_g^{1/2}\tilde{s}^{3/2}}{\overline{r}^{1/2}\tilde{Y}_{liq}^2}\left(\frac{2-\Lambda}{1-\Lambda}\right)\left[\overline{r}\tilde{Y}_{liq}(\overline{u}_{i,g}-\overline{u}_{i,l})\right]^{3/2} \qquad (13)$$

In this equation, C_D is a constant which should be found from comparison with measurements.

Figures 7 and 8 present results for axial slip velocity obtained with Eq. (13) compared with the measurements of [10]. These curves were obtained with C_D = 3.0. One can see, especially for the higher pressure, that the Eq. (13) predicts correct magnitude and trends for the slip velocity. In particular, the region occupied by smaller droplets would be characterized with very small slip velocity and this feature is reflected by Eq. (13). It is interesting to note that in some regions the liquid is moving faster than the gas and this point may deserve a further study.

CONCLUSIONS

The predictive capability of the Eulerian atomisation model [1] has been demonstrated for air-assisted atomisers. The influence of injector exit velocity profile, surface tension, gas velocity, and liquid and gas densities predicted by the model is in good agreement with experimental data.

A new transport equation for the slip velocity has been derived within the same Eulerian framework. The first application of this model for a typical coaxial air-water atomiser yields promising results.

NOMENCLATURE

D_t = turbulent diffusivity (m^2/s)
k = turbulent kinetic energy (m^2/s^2)
$\dot{m}_{vap}$ = vapour mass flow rate ($kg/s\ m^2$)
$\dot{m}$ = mass flow rate (kg/s)
R = universal ideal gas constant (8.341 J/kg K)
r = radial coordinate (m)
r_{eq} = droplet radius at equilibrium (m)
P = pressure (Pa)
Sc = Schmidt number, dimensionless
SMD = Sauter mean diameter (m)
T = temperature (K)
u_i, u_j = Cartesian velocity components (m/s)
$u_{i,g}$, $u_{j,l}$ = Cartesian components of gas and liquid velocities respectively (m/s)
x_i, x_j = Cartesian coordinates (m)
Y = mass fraction, dimensionless

Greek symbols

e = dissipation rate of turbulent kinetic energy (m^2/s^3)
h = surface tension (N/m)
L = time-averaged volume fraction of liquid
$= \overline{r}\tilde{Y}_{liq} / r_l$, dimensionless
r = density (kg/m^3)
s = interfacial area of liquid and gas per unit mass of the two-phase mixture (m^2/kg)
t_c = characteristic time for equilibrium (s)
n = kinematic viscosity (m^2/s)

Subscripts

eq = at equilibrium
g = of gas
l, liq = of liquid
m = of inter-phase momentum exchange
r = relative (between gas and liquid)
vap = of vapour
0 = at inlet

Superscripts

$\tilde{}$ = Favre averaged
$\bar{}$ = time averaged

REFERENCES

1. A. Vallet, A.A. Burluka and R. Borghi, Development of an Eulerian model for the atomisation of a liquid jet, *Atomization and Sprays*, vol. 11, pp. 619-642, 2001.
2. R.D. Reitz and F.V. Bracco, Mechanism of atomization of a liquid jet, *Phys. Fluids*, vol. 25, No. 10, pp. 1730-1742, 1982.
3. A. Lefebvre, Airblast atomization, *Progr. Energy Combust. Sci.*, vol. 6, pp. 233-261, 1980.
4. N. Beheshti, A.A. Burluka, M. Fairweather, Atomisation in turbulent flows: modelling for application, *Proc. Int. Symp. Turbulence and Shear FlowPhenomena*, vol.3, No. 2, pp. 619-624, 2003.
5. E.J. Hopfinger and J.C. Lasheras, Break-up of a water jet in high velocity co-flowing air, *Proc. ICLASS-94, Rouen, France*, pp. 100-117, 1994.
6. J.C. Lasheras, E. Villermaux and E.J. Hopfinger, Break-up and atomisation of a round water jet by a high speed annular air jet, *J. Fluid Mech.*, vol. 357, pp. 351-379, 1998.
7. L. Prevost, J.L. Carreau, E. Porcheron and F. Roger, Coaxial atomization under different ambient pressure, *Proc. ILASS-Europe'99*, pp. 251-256, 1999.
8. M. Madjid and I. Gokalp, A new correlation for turbulent mass transfer from liquid droplets, *Int. Heat Mass Transfer*, vol. 45, pp.37-45, 2002.